

Influence of Pressure-Equalizing Groove on Static Load Performance of Aerostatic Guideway

H. Zhang, X. Guan[†], T. Wang, A. U. Z. Robin and C. H. Mu

School of Mechanical and Power Engineering, Nanjing Tech University, Nanjing 211800, China
Jiangsu Province Key Laboratory of Industrial Equipment Manufacturing and Digital Control Technology,
Nanjing Tech University, Nanjing 211800, China

[†]Corresponding Author Email: 202061207101@njtech.edu.cn

(Received July 15, 2022; accepted January 11, 2023)

ABSTRACT

The load capacity and static stiffness of the existing air hydrostatic guideways are relatively low, and the static performance of the air film is degraded when external forces are increased during the process. Therefore, this study considered an aerostatic guideway of an ultra-precision micromachine tool as the research object. Single- and double-row orifice structures were designed on the guideway, and linear, extended, and X-shaped pressure-equalizing groove (PEG) structures with rectangular cross-sections were designed on the working surface of the guideway. By establishing a computational fluid dynamics model of the guideway air film, the pressure contour was obtained through simulation, and finally, the advantages of the double-row orifice structure were determined. Then, the influences of the structure, width, and depth of PEG and the diameter and number of orifices on the load capacity, stiffness, and air consumption were studied, which provided a theoretical basis for improving the load performance of the aerostatic guideway. The results showed that the design of the PEG effectively improved the load performance but increased the air consumption. The extended PEG exhibited the best load performance. When the eccentricity was large, the width of the PEG moderately increased, improving the load capacity and stiffness. While increasing the depth only improved the stiffness, it had little effect on the load capacity and air consumption. When the eccentricity was small, the diameter and number of orifices moderately increased. The experimental data were consistent with the simulation results, demonstrating the accuracy of the simulation method.

Keywords: Aerostatic guideway; Pressure-equalizing groove; Load capacity; Stiffness; Air consumption.

NOMENCLATURE

B	width of air film	l	vertical distance between two orifices
b_1	distance from orifice to left film edge	M	mass flow rate
b_2	distance from orifice to right film edge	n	orifice number
b_3	horizontal distance between two rows of orifices	P_d	outlet pressure
b_g	width of the pressure-equalizing groove	P_s	inlet pressure
d	orifice diameter	p	absolute pressure of gas
e	eccentricity	R	gas constant
F_{ij}	air film force	S	effective working surface area
G	bearing's gravity	T	absolute temperature of gas
h	air film thickness	u, v, w	gas velocities in x , y , and z directions
h_0	initial thickness of the air film	W	load capacity
h_g	depth of the pressure-equalizing groove	Δh	change of gas film thickness
h_o	orifice height	ΔW	change of load capacity
K	stiffness	μ	gas viscosity
L	length of air film	ρ	gas density

1. INTRODUCTION

With the rapid development of modern technology, certain fields, such as lasers, microelectronic equipment, aerospace, information engineering, and ultra-precision machining technology, have become the future development direction of product processing. Aerostatic bearings have high precision, fast response time, low heat generation, and no friction; thus, they have been widely used in essential equipment in ultra-precision manufacturing. Because air is used as a lubricating and supporting material in aerostatic bearings, externally pressurized air forms a thin film in the bearing, which provides the bearing load capacity, stiffness, and damping (Chang *et al.* 2015). Nonetheless, the compressibility of air makes it difficult to improve the load capacity and stiffness, which limits the application of aerostatic bearings (Cui *et al.* 2018). Recently, research on aerostatic bearings with high stiffness and load capacity has gained substantial attention from scholars. Many scholars started from the theory of fluid lubrication and improved and optimized the theoretical equation according to the specific bearing structure. This yielded improved calculation accuracy and avoided the calculation error caused by model simplification. The load capacity, stiffness, and stability of the air film were enhanced by the improved orifice restrictors and pressure-equalizing groove (PEG) structures.

Lu *et al.* (2020) solved the governing equation of aerostatic bearings in a multi-hole integrated orifice restrictor using the finite difference method (FDM) and flow balance principle in Cartesian coordinates. The calculation results showed that the number and diameter of orifices substantially influence the load capacity and stiffness. Gao *et al.* (2015) designed six orifice chamber structures with different shapes on the aerostatic bearings of an ultrahigh-speed spindle and calculated the load performance of the bearings using the computational fluid dynamics method. Furthermore, the experimental results agreed with the computational fluid dynamics results. Nishio *et al.* (2011) used FDM to study the static and dynamic characteristics of aerostatic thrust bearings. They found that the stiffness and damping coefficient of bearings with small orifices are better than those of bearings with compound orifices, and the roughness of the bearing surface significantly influences the performance. Lai *et al.* (2019) combined magnetic error feedback with grid parameter optimization to solve a hydrostatic guideway model; analyzed the influence of the diameter, number, and distribution of orifices on load performance; optimized the layout of a perforated plate; and experimentally determined the best position of the perforated plate. Aoyama *et al.* (2006) designed an orifice restrictor with a round corner outlet. Through simulation and experimental analysis, it was found that, compared with an orifice with a 90-degree angle outlet, the orifice with a round outlet could restrain bearing vibrations. Xiao *et al.* (2018) studied the effects of constraints, structures, operating parameters, and pneumatic pressure on the performance of aerostatic radial microbearings and conducted experiments on prototype bearings to verify a numerical model. Zhang *et al.* (2018) used

the separated variable method (MSV) to solve laminar boundary layer equations to analyze the effects of film thickness, orifice diameter, and air supply pressure on the radial pressure distribution and static performance of bearings. Sahto *et al.* (2020) modeled and simulated porous, single-orifice, and multiple-orifice types of porous, orifice, and multiple categorized of aerostatic thrust bearings. Through numerical analysis and experience, the influences of materials, geometric factors, film thickness, and air supply pressure on the load capacity and stiffness of three bearings were analyzed.

In addition to optimizing orifices, a PEG structure can be designed on the working face of aerostatic bearings, and the load performance can be improved by changing the gas film pressure distribution. Yan *et al.* (2019) studied the influence of three different groove-shaped PEG bearings and bearings without PEG on their dynamic characteristics under different working conditions. The results show that triangular and trapezoidal groove bearings have apparent advantages under different working conditions. Gao *et al.* (2019) analyzed the influence of different groove numbers, groove depths, and air supply pressures of herringbone PEG on the aerostatic sliding bearings of an ultra-high-speed spindle using the improved finite element method. Research shows that proper geometric parameters of herringbone grooves can reduce the radial runout of spindles. Du *et al.* (2014) systematically studied the influence of factors, such as the number, position, and size parameters of PEG, on the load performance of aerostatic bearings. Through simulations and experiments, it was found that circumferential and axial PEGs significantly impact the load performance. Guenat and Schiffmann (2019) designed a spiral groove on the foil of gas foil thrust bearings to improve the bearing load capacity and reduce the resistance torque. Based on the gas-solid coupling principle. Zhao *et al.* (2017) studied the influence of elastic PEG on the stiffness of aerostatic thrust bearings under different gas film gaps, and experimentally verified the feasibility of the gas-solid coupling method. Chen and Lin (2002) designed an X-shaped PEG aerostatic bearing. The Newmark integral method and improved resistance network method (RNM) were used to analyze the influence of the X-shaped PEG on the static characteristics and dynamic stability of the bearings under different structural parameters, and the applicability of the RNM method was verified experimentally.

In summary, to date, research on PEG has mainly focused on hydrostatic rotary thrust and radial bearings, and small number of air inlets. There is still a lack of research on PEGs of linear axis hydrostatic guideways with large numbers and multiple rows of air inlets. The shape, type, and size of PEGs for this type of guideway are systematically limited to static performance. Therefore, in this study, an aerostatic guideway for an ultra-precision micro-numerical control machine tool was considered as the research object. When the working face of the aerostatic guideway adopts a single row of orifices, a linear

PEG is designed. Three types of PEG structures (linear, extended, and X-shaped) with double rows of orifices were designed. On research methods, Siddiqui *et al.* (2022) used the computational fluid dynamics (CFD) method, COMSOL, and MATLAB software to predict the temperature drop of plain finned tube heat exchangers under different inlet conditions. They also discussed the significant influence of air flowrates on dry heat transfer and the relationship between fin-pitch structure and air humidity. They found that the effect of multirow heat exchangers is better than that of a single row. Shah *et al.* (2022) explored the cooling performance of low-concentration Fe2O3/water and selected three concentrations, three inlet temperatures, and five flow rates to study and obtain relationships. Ejaz *et al.* (2022) used the fluid volume provided by ANSYS Fluent, which is a multiphase model, to simulate and analyze air-water slug flow with eight different velocity ratios in five diverging T-junctions. Therefore, this study adopted similar research methods and ideas, established the CFD model, and simulated and calculated the load capacity, stiffness, and mass flow rate of the air film in a guideway without and with different PEG structures using the laminar flow model in ANSYS Fluent, and determined the optimal orifice distribution and PEG structure. Furthermore, the impacts of the width and depth of the grooves and the quantity and diameter of the orifices on the overall load performance were studied. This study is important for the design of aerostatic guideways. Finally, the influence of different air supply pressures on the performance of a guide rail was measured experimentally, and the accuracy of the numerical analysis was verified.

2. STRUCTURE AND PARAMETERS

A simplified stress model of an aerostatic guideway is shown in Fig. 1 and is mainly composed of a guideway and slider. The high-pressure gas produced by an external air source equipment is introduced into multiple air passages inside the slider of the aerostatic guideway through the air inlet and enters the lubrication gap between the slider and guideway after flowing through the orifice and PEG, forming a thin film with load capacity and stiffness, thus lubricating the guideway and supporting the external load. Finally, the gas flowed out from the end of the guideway.

Under the bearing's gravity G , external load W , and air film forces F_{ij} generated by six air films, the air film forces acting on the load capacity are F_{11} , F_{12} , F_{31} , and F_{32} , where F_{31} and F_{32} are in the same direction as the gravity, whereas F_{11} and are opposite to the direction of the gravity. To ensure the guideway load capacity, $W = F_{11} + F_{12} - F_{31} - F_{32} - G$ is required. To improve F_{11} and F_{12} and the load capacity W , rectangular PEGs were designed at the outlets of the orifices at the top of the slider. Considering the air film with six orifices evenly distributed as an example, the initial thickness of the air film was $h_0 = 20 \mu\text{m}$. A film

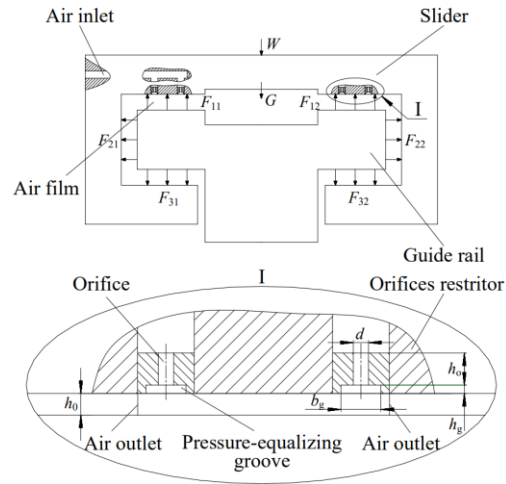


Fig. 1. Simplified model and stress model of the aerostatic guideway.

structure with a single-row orifice is shown in Fig. 2(a), and a film structure with a double row of orifices is shown in Fig. 2(b). The four types of PEG structure were linear, extended, X-shaped, and without PEG. The film structures on both sides of the slider were entirely symmetrical, and the basic dimensional parameters of the air film are listed in Table 1.

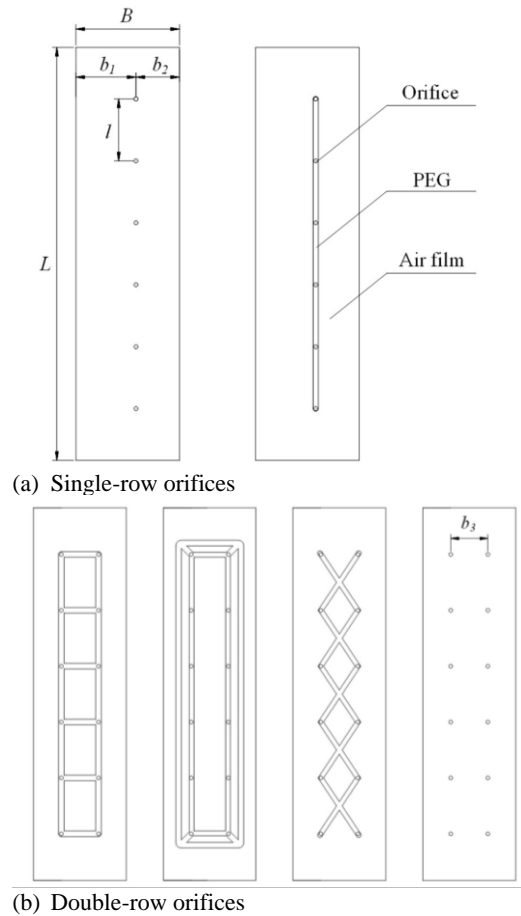


Fig. 2. Air film structures with single-row or double-row orifices restrictors.

Table 1 Dimensions of the air film

Film location	<i>L</i>	<i>B</i>	<i>b</i> ₁	<i>b</i> ₂	<i>b</i> ₃	<i>l</i>
Top /mm	260	37	24	13	13	44
Bottom /mm	260	40	24	16	14	44

3. GOVERNING EQUATION

To solve the pressure distribution on the film surface, the capacity, stiffness, and mass flow rate of the film were calculated with the following assumptions (Chen and He 2006).

1. The internal gas is Newtonian fluid and conforms to Newton's law of motion.
2. The internal gas is a single-phase and continuous medium.
3. The internal gas in the flow process is at a moderate temperature.
4. The mass flow rates of the gas flowing into and out of the gas film are equal.
5. The flow pattern is laminar flow.

The continuity equation for compressible fluids is described in Eq. (1) (Shao *et al.* 2018).

$$\frac{\partial \rho}{\partial h_g} + \frac{\partial(\rho u)}{\partial x} + \frac{\partial(\rho v)}{\partial y} + \frac{\partial(\rho w)}{\partial z} = 0 \quad (1)$$

where ρ is the gas density, h_g is the height of the cross-section of the PEG, u , v , and w are the velocities of the gas in x , y , and z directions, respectively.

The equation for the isothermal gas state is described in Eq. (2) (Yan *et al.* 2019).

$$\frac{p}{\rho} = gRT \quad (2)$$

where p is the absolute pressure of the gas, R is the gas constant, g is the acceleration owing to gravity, and T is the absolute temperature of the gas.

The simplified Reynolds equation for a laminar gas flow is given by Eq. (3) (Grassam *et al.* 1965).

$$\frac{\partial}{\partial x} \left(\frac{\rho h^3}{\mu} \frac{\partial p}{\partial x} \right) + \frac{\partial}{\partial y} \left(\frac{\rho h^3}{\mu} \frac{\partial p}{\partial y} \right) = 0 \quad (3)$$

where h is the film thickness, and μ is the viscosity of the gas.

The load capacity of the gas film was calculated using Eq. (4) (Bassani and Piccigallo 1992).

$$W = \int_S p dS \quad (4)$$

where S is the effective working surface area of the aerostatic guideway, that is, the gas film area at the top and bottom of the guideway.

When the guideway is subjected to an external load, the film thicknesses at the top and bottom of the guideway will have an exact size change; the top film becomes thinner under pressure, and the bottom film becomes thicker. Assuming that the change in thickness of the gas film is Δh , the stiffness of the guideway under different eccentricities e can be obtained. Filtered air was used as the gas in this study.

The equation of eccentricities e is shown in Eq. (5) (Bassani and Piccigallo 1992).

$$e = \frac{\Delta h}{h} \quad (5)$$

The stiffness is defined in Eq. (6) (Bassani and Piccigallo 1992).

$$K = \frac{\Delta W}{\Delta h} \quad (6)$$

4. SIMULATION ANALYSIS

4.1 Setting of Boundary Conditions

In this study, PEGs were designed on the working surface of guideways based on single-row and double-row orifice restrictors, and the influence of the PEGs on static performance was studied. We considered an extended PEG guideway with 12 orifices as an example. The air film model is illustrated in Fig. 3. In this study, the Fluent module in ANSYS Workbench was used to simulate the air film, and a laminar flow model was used as the calculation model. The air

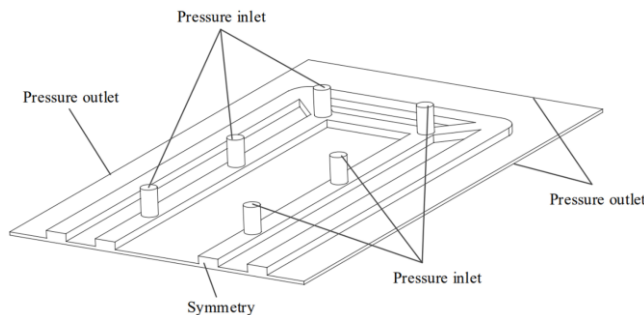


Fig. 3. Air film simulation model.

film was symmetrical. Half of the air film was used in the simulation calculation to improve the calculation speed. The air film inlet was set as the pressure inlet, and the inlet pressure was $P_s = 0.5 \text{ MPa}$. The air film outlet was set as the pressure outlet, and the outlet pressure was $P_d = 0.1 \text{ MPa}$. The air film section was set as a symmetrical surface, the other surfaces were set as wall surfaces. The simulation model adopts laminar flow model, and the other parameters were set as default parameters.

4.2 Single- and Double-Row Orifices

The high-pressure air flowing out of the orifices was throttled twice by designing a PEG structure at the orifices, and the pressure distribution of the air film was improved. However, the distribution of the orifices directly affected the distribution range of the high-pressure zone of the film. This section presents the influence of single- and double-row orifices and the corresponding PEG structures on the static performance of the guideway.

The influence of PEG on the load capacity of the aerostatic guideway was studied when the orifices were distributed in a single row, and an air film model with and without grooves was simulated and calculated. The structural diagram of the model is shown in Fig. 2(a), the basic dimensions of which are shown in Table 1, and the air film pressure distributions with and without PEG are shown in Fig. 4(a).

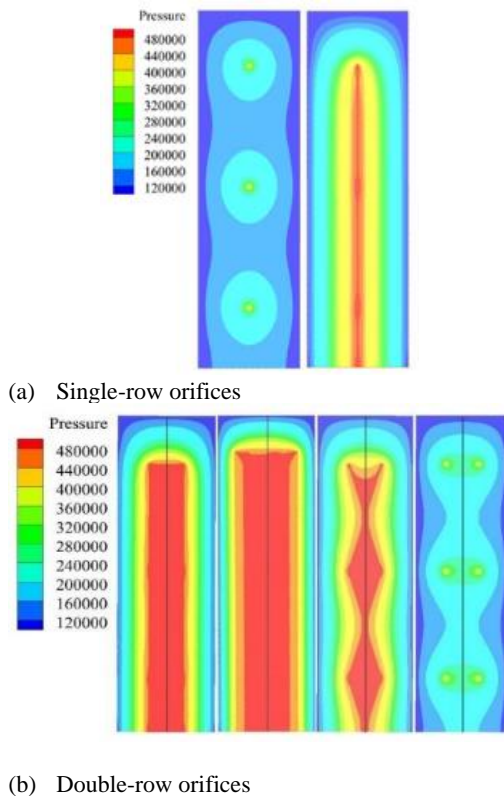


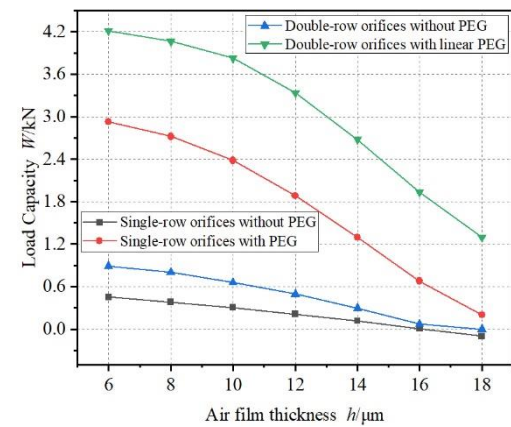
Fig. 4. Air film pressure contours of single- and double-row orifice restrictors.

As shown in Fig. 4(a), compared with the guideway without a groove, the air film pressure in the guideway with a groove was higher, the pressure distribution was more uniform, and the pressure drop tended to be gentler.

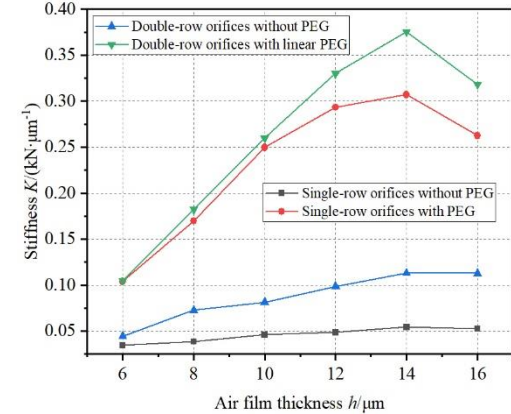
The influence of PEG on the load capacity of the aerostatic guideway was studied when the orifices were distributed in double rows. Air film models with linear, extended, and X-shaped PEGs and those without a PEG were simulated and calculated. The structural diagram of the model is shown in Fig. 2(b), the basic dimensions of which are shown in Table 1, and the simulated air film pressure distributions of the four types of PEG are shown in Fig. 4(b).

As shown in Fig. 4(b), compared with the guideway without a groove, the film pressure of the guideway with a groove was substantially increased, the range of the high-pressure zone was apparently enlarged, and the pressure distribution was more uniform, in which the high-pressure zone of the extended PEG guideway was the largest. Therefore, the design of the equalizing groove structure effectively reduced the film pressure drop and improved the load capacity.

The load performance of the aerostatic guideway with single-row and double-row orifices, with and without PEG, was calculated. Both single- and double-row PEG structures used the linear type, as an example. Results of the comparative analysis of



(a) Load capacity



(b) Stiffness

Fig. 5. Load performances of guideways with single- and double-row orifices.

the load performance were obtained and shown in Fig. 5.

Figure 5 shows that the load capacity of the air film decreased with an increase in the film thickness. This was because a larger air film thickness sped up the passage of high-pressure air through the guideway gap, increasing the outlet range and reducing the air outflow resistance, resulting in a decrease in the film surface pressure, which led to a decrease in the load capacity. The maximum load capacity of the air film of single-row orifices was 1350 N, and the maximum stiffness was 16.3 N/μm, whereas the maximum load capacity of double-row orifices was 1660 N, and the maximum stiffness was 40 N/μm. The air film load capacity and stiffness of the double-row orifices increased by 23% and 145%, respectively, compared to those of the single-row orifices. Therefore, the guideway with double-row orifices had better load performance under normal working conditions than that with the single-row orifices.

The above analysis proved that adding pressure-equalizing grooves can effectively reduce the air film pressure drop and improve the load capacity of aerostatic guideways. The results also show that distributing the orifices in double rows is better than in single rows. Subsequently, the influence of the structures and size parameters of PEGs on the load performance was further analyzed when the orifices were distributed in a double row.

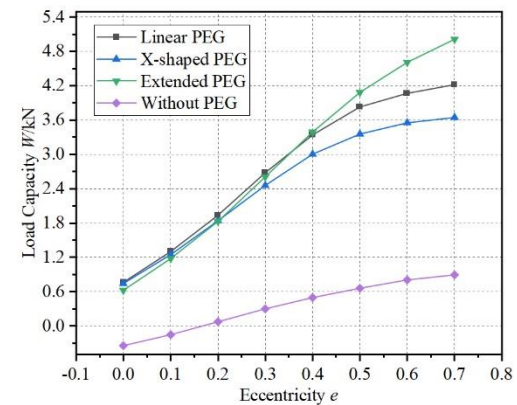
4.3 Influence of PEG Structure on Load Performance

Under the conditions of groove depth $h_g = 0.2$ mm , width $b_g = 0.4$ mm , orifice diameter $d = 0.2$ mm , height $h_o = 0.5$ mm , number $n = 12$, inlet pressure $P_s = 0.5$ MPa , and outlet pressure $P_d = 0.1$ MPa , the linear, extended, and X-shaped PEG guideways, and guideways without PEG were analyzed under different eccentricities. Eccentricity is the ratio of the change in air film thickness to the initial air film thickness after the load of the hydrostatic guideway changes; the specific formula is shown in Eq. (5).

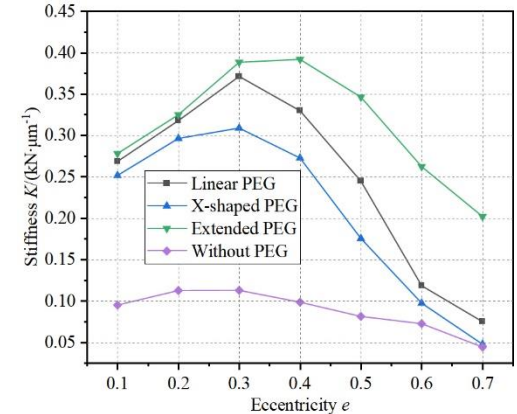
Figure 6(a) shows that with an increase in eccentricity, the load capacity gradually increases, indicating that the thinner the air film, the better the PEG can improve the load capacity, and the more significant was the effect of the extended groove. When the eccentricity was $e < 0.4$, the load capacity of the linear groove was slightly larger than those of other groove guideways, and when $e \geq 0.4$, the extended groove guideway exhibited the best effect. The load capacities with PEGs were relatively larger than that without a PEG. When the eccentricity was small, the load capacity without a PEG was negative.

Figure 6(b) shows that when eccentricity increased, the stiffness first increased and then decreased. The maximum stiffness of all guideways with PEGs

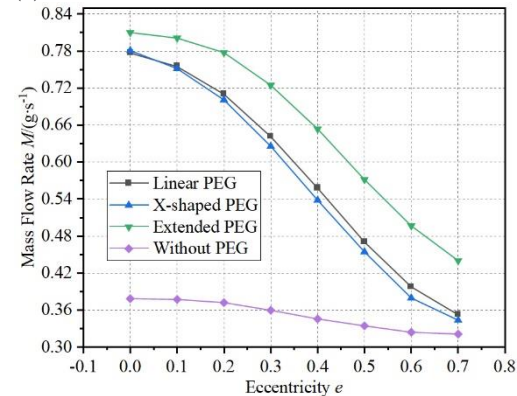
appeared near the eccentricity $e = 0.3$, and the stiffness value of the extended groove was the highest, which indicates that there was an optimal eccentricity range. The maximum stiffness of the extended groove guideway was approximately 4.3 times that of the guideway without a groove. When the eccentricity $e \leq 0.3$, the stiffness values of the extended and linear grooves were not substantially different. When the eccentricity $e > 0.3$, the advantage of the extended groove was apparent. When considering the load capacity and stiffness, the optimal eccentricity was generally between 0.3 and 0.6.



(a) Load capacity



(b) Stiffness



(c) Mass flow rate

Fig. 6. Effect of PEG structure on load performance

Figure 6(c) shows that the air consumption decreased with an increase in eccentricity. The air consumption of the guideways with PEGs was the largest, whereas those of the guideways with linear and X-shaped grooves differed slightly. Compared with the air consumption of guideways without PEG, those with PEG structures had higher air consumption by two times.

In summary, the PEG designs effectively improved the air film load capacity and stiffness, among which the extended design had the best effect on stiffness and load capacity; however, the air consumption increased accordingly.

4.4 Influence of PEG Width on Load Performance

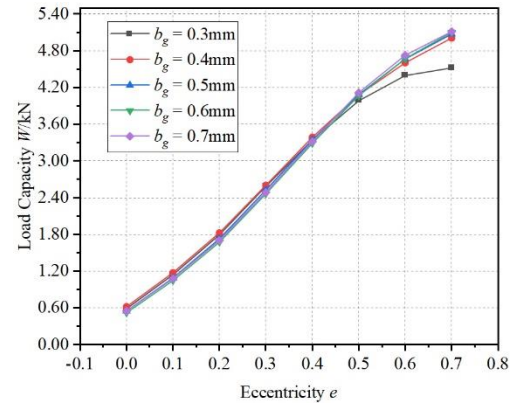
Upon analyzing the results presented in the previous section, it can be concluded that the extended groove had the best effect on the improvement of the load capacity and stiffness; however, compared with guideways without a PEG, the PEGs extended the extent of the air film, resulting in higher air capacity in the air film, which caused vibrations in the guideways. Therefore, the size of the PEG should be as small as possible to meet the usage requirements. Therefore, with a PEG depth of $h_g = 0.2$ mm and the other conditions remained unchanged, the changes in load capacity, stiffness, and air consumption when the widths of the extended groove were 0.3, 0.4, 0.5, 0.6, and 0.7 mm were analyzed. The simulation results are shown in Fig. 7.

Figure 7(a) shows that When the eccentricity was maintained at $e < 0.4$, the width of the PEG had no evident influence on the load capacity, and when the PEG width was $b_g = 0.4$ mm, the load capacity slightly increased, whereas when the width was $b_g = 0.7$ mm, the load capacity slightly decreased, indicating that the wider the PEG, the larger the decrease in the load capacity. When $e \geq 0.4$, the load capacity at width $b_g = 0.7$ mm was more significant than at other widths, whereas the load capacity at width $b_g = 0.3$ mm was the smallest, indicating that when eccentricity is large, increasing the width of the PEG can improve the load capacity.

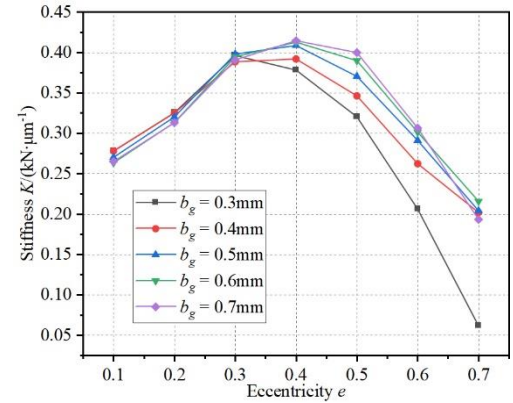
Figure 7(b) shows that the stiffness of the guideways with different PEG widths reached a peak when the eccentricity was $e = 0.4$. When the eccentricity was maintained at $0.1 < e \leq 0.2$, the smaller the PEG width, the greater the stiffness, indicating that when the eccentricity is low, a narrower PEG width can effectively increase the stiffness.

Figure 7(c) shows that under the same eccentricity, the air consumption of the guideway increased with an increase in the width of the PEG, and when the width of the PEG reached 0.5 mm or higher, the groove width had little effect on the air consumption.

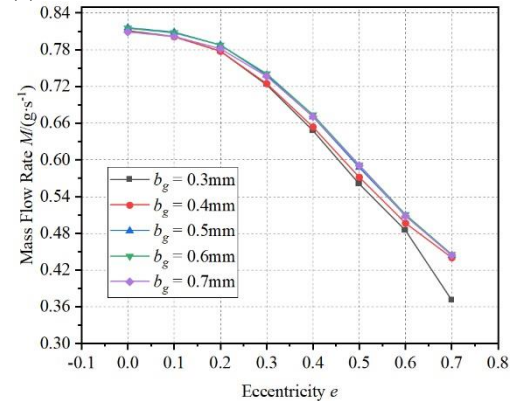
In summary, increasing the width of the PEG improved the load capacity of the air film; however,



(a) Load capacity



(b) Stiffness



(c) Mass flow rate

Fig. 7. Effect of PEG Width on Load Performance.

the effect was limited. When the eccentricity was between 0.4 and 0.7, the stiffness of the air film decreased significantly when the width of the air film was reduced, and the overall air consumption of the guideway remained relatively constant.

4.5 Influence of PEG Depth on Load Performance

The influence of PEG depth on the static performance was analyzed for the PEG width $b_g = 0.4$ mm, with other conditions maintained constant. When the depths h_g of the extended groove were 0.2, 0.25, 0.3, 0.35, and 0.4 mm, the changes in load capacity, stiffness and, air consumption were

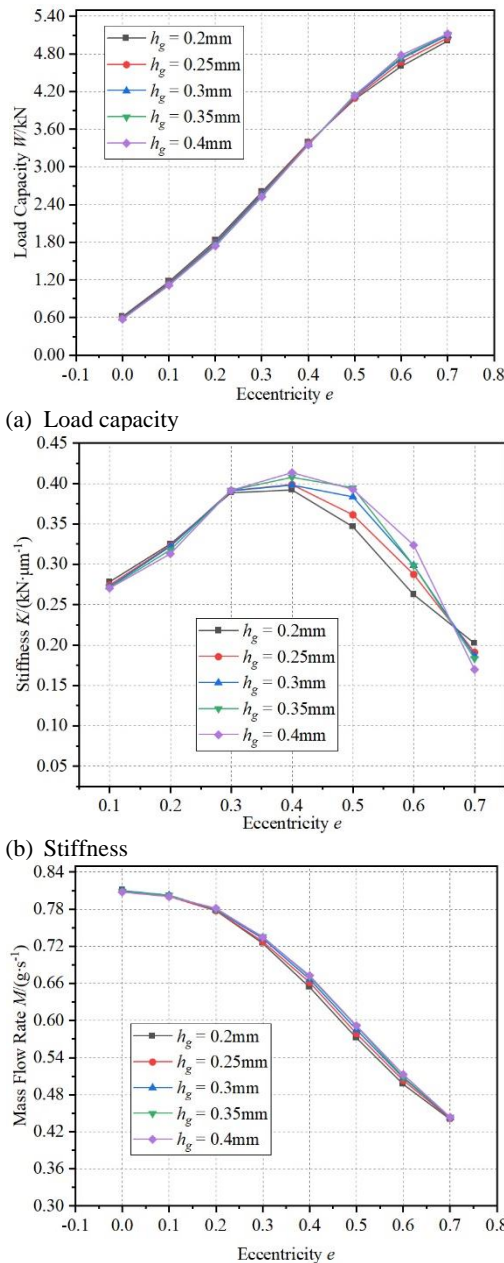


Fig. 8. Effect of PEG depth on load performance.

evaluated or analyzed. The simulation results are shown in Fig. 8.

Figure 8(a) shows that when the eccentricity was maintained at $e \leq 0.5$, changes in PEG depths had no apparent influence on the load capacity; When the eccentricity was $e > 0.5$, the load capacity increased slightly with the increase in PEG depth.

As shown in Fig. 8(b), when the eccentricity was maintained at $e \leq 0.3$, the PEG depth had little influence on the guideway stiffness, and the larger the groove depth, the smaller the stiffness. When the eccentricity was $0.3 < e < 0.7$, the PEG depth had a significant influence on the stiffness. The larger the groove depth, the larger the stiffness. The stiffness at different groove depths reached a peak when the

eccentricity was $e = 0.4$. It increased the stiffness effectively by moderately increasing the depth of the PEG. When the eccentricity was $e = 0.7$, the larger the groove depth, the smaller the stiffness because when the groove depth increased to a specific value, the PEG increased the air film pressure, which caused instability of the air film.

As shown in Fig. 8(c), when the eccentricity was maintained at $0.3 < e < 0.7$, a moderate increase in the groove depth slightly increased the mass flow rate; however, the effect was not apparent. Generally, the depth of the PEG had little influence on the load capacity and air mass flow rate.

In summary, the depth of the PEG had no evident influence on the air film load capacity, stiffness, and air consumption. When the eccentricity was between 0.4 and 0.6, increasing the depth slightly improved the stiffness.

4.6 Influence of the Orifice Diameter on Load Performance

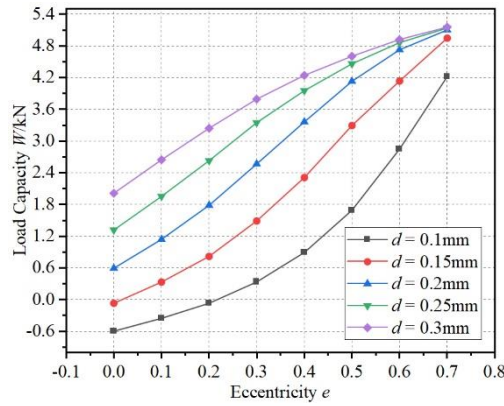
The influence of orifice diameter on static performance was analyzed for groove depth $h_g = 0.2\text{ mm}$, width $b_g = 0.4\text{ mm}$, orifice height $h_o = 0.5\text{ mm}$, number $n = 12$, inlet pressure $P_s = 0.5\text{ MPa}$, and outlet pressure $P_d = 0.1\text{ MPa}$. The changes in load capacity, stiffness, and air consumption were studied for orifice diameter values of 0.1, 0.15, 0.2, 0.25, and 0.3 mm. The simulation results are shown in Fig. 9.

As shown in Fig. 9(a), the load capacity increased with eccentricity. Under the same eccentricity, increasing the orifice diameter effectively improved the load capacity. The load capacities of different orifice diameters were remarkably different when the eccentricity was small. When the eccentricity increased to 0.7, except for $d = 0.1\text{ mm}$, the load capacity corresponding to the other orifices exhibited little difference.

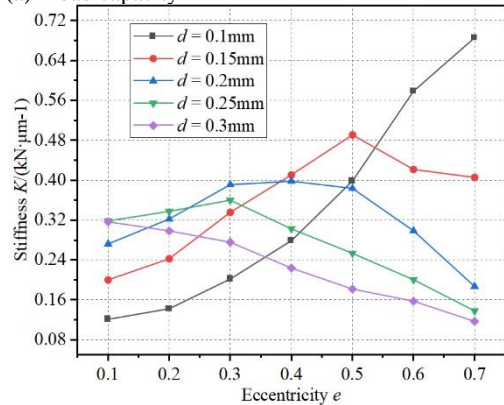
Figure 9(b) shows that with the increase in eccentricity, the stiffness increased when $d = 0.1\text{ mm}$. The stiffness decreased when $d = 0.3\text{ mm}$. When the eccentricity was $e < 0.3$, the stiffness moderately increased by increasing the diameter of the orifices. When eccentricity was $e > 0.5$, the diameter of the orifice had a significant influence on stiffness; the larger the diameter, the smaller the stiffness.

As shown in Fig. 9(c), under the same eccentricity, the larger the orifice diameter, the greater the air consumption, and when the eccentricity was small, the influence was significant. However, with the increase in eccentricity, the influence of the orifice diameter on the air consumption gradually decreased, and when the eccentricity was $e = 0.7$, it had almost no effect.

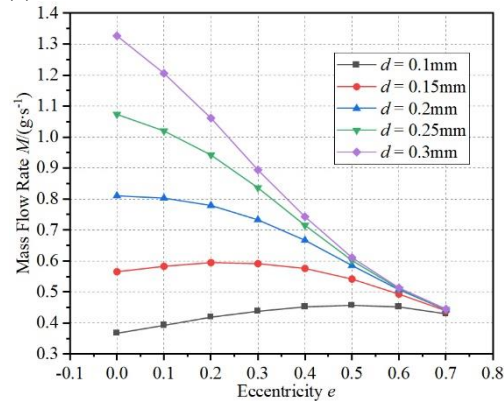
In summary, when the eccentricity was small, a larger-diameter orifice improved the load capacity;



(a) Load capacity



(b) Stiffness



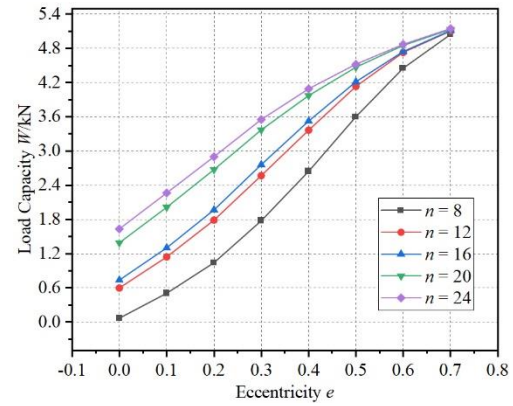
(c) Mass flow rate

Fig. 9. Effect of orifice diameter on load performance.

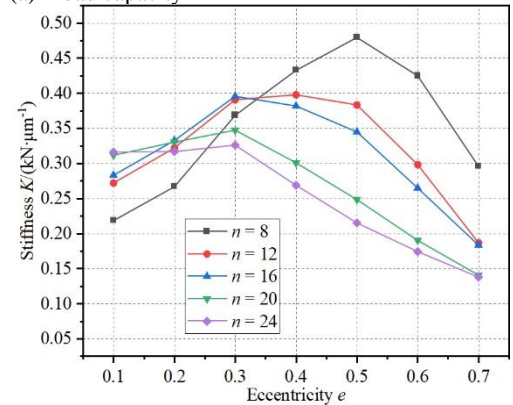
however, the air consumption increased significantly. However, the lifting effect decreased with an increase in the eccentricity. Therefore, to obtain larger stiffness, it is necessary to design the orifice diameter according to the film thickness of the guideway.

4.7 Influence of Orifice Number on Load Performance

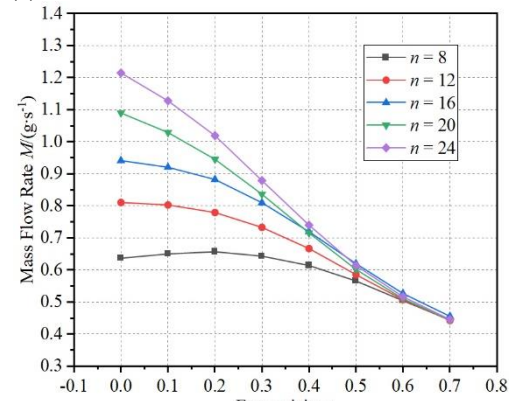
The influence of the number of orifices on the static performance for orifice diameter $d = 0.2 \text{ mm}$, with other conditions maintained constant, was analyzed. In addition, the changes in the load capacity, stiffness, and air consumption when the numbers of



(a) Load capacity



(b) Stiffness



(c) Mass flow rate

Fig. 10. Effect of orifice number on load performance.

orifices were 8, 12, 16, 20, and 24 were evaluated. The simulation results are shown in Fig. 10.

Figure 10(a) indicates that under the same eccentricity, the larger the number of orifices, the greater the load capacity. With an increase in eccentricity, the improvement in load capacity caused by increasing the number of orifices gradually decreased. When eccentricity was $e = 0.7$, the number of orifices had little effect on the load capacity.

Figure 10(b) shows that the smaller the orifice number, the larger the influence of eccentricity on stiffness, particularly when $n = 8$. When the eccentricity was maintained at $e < 0.2$, moderate

increase in the orifice number improved the stiffness; however, when $n \geq 20$, the stiffness decreased slightly. When the eccentricity was $0.2 < e < 0.4$, moderately reducing the orifice number positively impacted the stiffness. When the eccentricity was $e \geq 0.4$, increasing the orifice number weakened the stiffness, and when eccentricity was $h = 8$, the stiffness with an orifice number of $h = 8$ reached the maximum.

As shown in Fig. 10(c), under the same eccentricity, the larger the number of orifice, the higher is the air consumption. With an increase in eccentricity, the influence of the orifice number on air consumption gradually decreased. When $e > 0.5$, the orifice number had little effect on the air consumption; however, increasing the orifice number caused a slight decrease in the air consumption. An orifice number of $n = 16$ resulted in the largest air consumption.

In summary, the effect of orifice number on the air film performance was similar to that of orifice diameter. Increasing the orifice number improved the load capacity but weakened the stiffness and increased the gas consumption.

5. EXPERIMENT

5.1 Experiment Setup

The experimental object was an aerostatic guideway, as illustrated in Fig. 11. The load capacity and air film gap of the guideway under different air supply pressures were measured to determine the stiffness under these supply pressures. The experimental equipment mainly included air filtering equipment, cylinder loading equipment, digital screen tension meter, aerostatic guideway, micro-displacement measuring equipment, testing platform, and marble optical platform, as shown in Fig. 12. The entire setup was placed on a marble optical platform. The high-pressure air for the aerostatic guideway was obtained using a centralized air supply system in the laboratory. After passing through the three-stage air

filter and being adjusted to the required pressure by a pressure-regulating valve, the high-pressure air entered the aerostatic guideway, resulting in a film gap. The external air source was connected to the cylinder through a pressure-regulating valve to provide a load for the guideway. The output force was displayed using a digital screen tension meter. The air film gap changes under different loading forces were measured by placing a micro-displacement sensor on the surface of the slider. By using the average value of the experimental data collected at several locations under the same air supply pressure, random errors were eliminated, and the connection between the load capacity and film thickness of the aerostatic guideway under various air supply pressures was achieved. To eliminate random errors, the relationship between the load capacity and film thickness of the aerostatic guideway under different air supply pressures was obtained by calculating the average value of the experimental data at different positions under the same air supply pressure. The experimental data were then analyzed to obtain a stiffness curve that was compared with the simulation results.

The experimental aerostatic guideway and air film sizes were similar to those used in the simulation model. The air guideway had an orifice number of $n = 39$, diameter of the orifice was $d = 0.1 \text{ mm}$, and initial thickness of the air film was $h_0 = 15 \text{ }\mu\text{m}$.

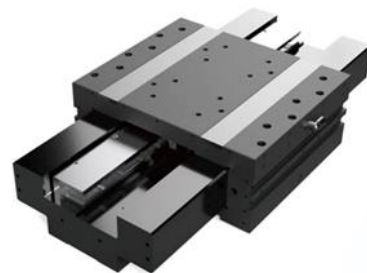


Fig. 11. Experimental model of air aerostatic guideway

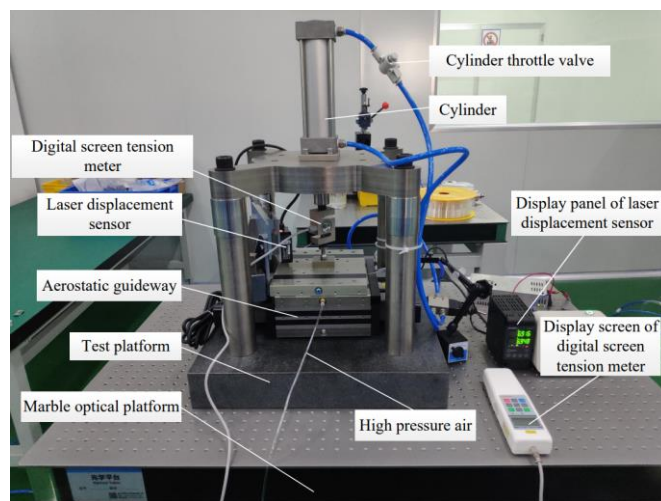
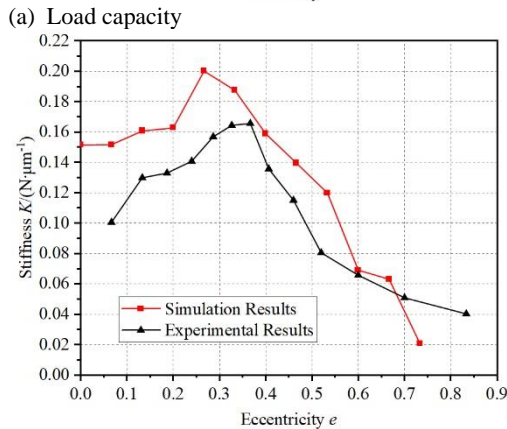
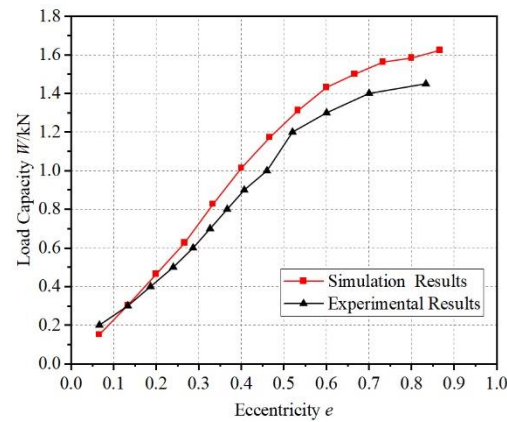


Fig. 12. Experiment setup.

5.2 Experimental Results

Figures. 13(a) and 14 show that the load capacities obtained by the experiments and simulation exhibited the same trend; they increased with an increase in eccentricity. The load capacity measured in the aerostatic guideway test was less than the calculated value. The results show that the error between the calculated and experimental load capacities was less than 12%. With an increase in eccentricity, the difference between them gradually increased. This was because when the eccentricity was larger, the film thickness was smaller, and the guideway surface roughness significantly influenced the experimental results, which led to a reduction in the load capacity. However, the guideway surface roughness had little influence when the film thickness was large.

Figures. 13(b) and 14 show that the experimental and calculated stiffness exhibited similar trend. The measured stiffness of the aerostatic guideway was less than the calculated stiffness. This was because of the calculation formula adopted in this study for stiffness. When the air film thickness was large, the air film of the guideway shifted easily, resulting in a wedge-shaped gap and a dynamic pressure effect, which was different from the theoretical simulation value of a parallel gap. Therefore, the smaller the eccentricity, the larger the difference between them.



(a) Load capacity
(b) Stiffness
Fig. 13. Comparison of experimental and simulation results at 0.4 MPa supply pressure.

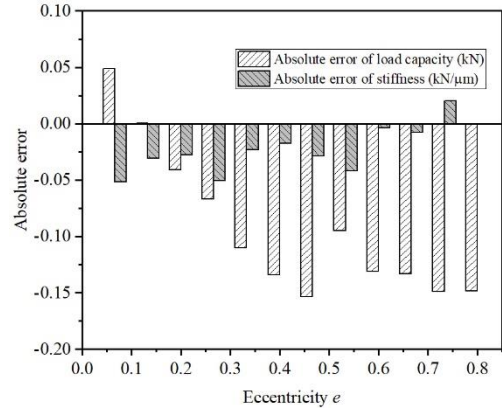


Fig. 14. The absolute error of experimental data and simulation data of load capacity and stiffness.

The measurement error of stiffness was larger when the film thickness was larger.

Owing to the limitations of the experimental conditions, there were some external interferences in the experimental process, which inevitably led to some errors between the experimental results and simulation data. However, the data were within a specific range of errors and coincided with each other, which proved the rationality of the simulation model and the accuracy of the calculated results obtained in this study.

6. CONCLUSIONS

(1) Based on the CFD simulation method, the static performance of the aerostatic guideway of an ultra-precision micromachine tool with single- and double-row orifice structures and linear, extended, and X-shaped pressure-equalizing groove (PEG) structures was analyzed, and the feasibility of the simulation model was verified experimentally.

(2) Through this research, it was found that the design of the PEG structure could effectively make the air film pressure distribution more uniform, reduce the pressure drop, and improved the load capacity and stiffness. In comparison, it was found that the static performance of the extended groove guideway was the best. The influence of each parameter was determined through systematic research. It was found that the structural parameters of the extended groove had little influence on the static performance; however, the orifice parameters and number had significant influences. When the film thickness changed significantly, increasing the diameter and number of orifices improved the load capacity and stiffness. In addition, increasing the input of clean air increased the energy consumption

(3) The extended PEG was a combination of multiple rectangular grooves, which was less difficult to process compared to other arc grooves. Therefore, a hydrostatic guideway with an extended and double-row orifice PEG structure, combined with the static performance of an air film, was more suitable for small machine tools.

(4) This study provides a particular reference model for the optimization design of an air aerostatic guideway with a pressure-equalizing groove, the determination of structural parameters, and air film thickness under specific working conditions. However, the optimal combination of various parameters of extended PEG and the dynamic performance of the air film still need to be explored.

ACKNOWLEDGEMENTS

This work was supported by the National Natural Science Foundation of China (Grant No. 51205211), and the Natural Science Foundation of Jiangsu (Grant No. BK20190676).

REFERENCES

- Aoyama, T., Y. Kakinuma and Y. Kobayashi (2006). Numerical and experimental analysis for the small vibration of aerostatic guideways. *CIRP annals* 55 (1), 419-422.
- Bassani, R. and B. Piccigallo (1992). *Hydrostatic lubrication*. Elsevier, Amsterdam, Netherlands.
- Chang, S. H., C. W. Chan and Y. R. Jeng (2015). Discharge coefficients in aerostatic bearings with inherent orifice-type restrictors. *Journal of Tribology* 137 (1), 011705.
- Chen, M. F. and Y. T. Lin (2002). Static behavior and dynamic stability analysis of grooved rectangular aerostatic thrust bearings by modified resistance network method. *Tribology International* 35 (5), 329-338.
- Chen, X. D. and X. M. He (2006). The effect of the recess shape on performance analysis of the gas-lubricated bearing in optical lithography. *Tribology International* 39 (11), 1336-1341.
- Cui, H. L., Y. Wang, B. R. Wang, H. Yang and H. Xia (2018). Numerical simulation and experimental verification of the stiffness and stability of thrust pad aerostatic bearings. *Chinese Journal of Mechanical Engineering* 31 (1), 1-12.
- Du, J. J., G. Q. Zhang, T. Liu and S. To (2014). Improvement on load performance of externally pressurized gas journal bearings by opening pressure-equalizing grooves. *Tribology International* 73, 156-166.
- Ejaz, F., W. Pao and H. M. Ali (2022). Numerical investigation and prediction of phase separation in diverging T-junction. *International Journal of Numerical Methods for Heat & Fluid Flow* 32 (12), 3671-3696.
- Gao, S. Y., K. Cheng, S. J. Chen, H. Ding and H. Y. Fu (2015). CFD based investigation on influence of orifice chamber shapes for the design of aerostatic thrust bearings at ultra-high speed spindles. *Tribology International* 92, 211-221.
- Gao, S. Y., Y. G. Shi, L. S. Xu, H. Chen and K. Cheng (2019). Investigation on influences of herringbone grooves for the aerostatic journal bearings applied to ultra-high-speed spindles. *Proceedings of the Institution of Mechanical Engineers Part C-Journal of Mechanical Engineering Science* 233 (16), 5795-5812.
- Grassam, N., R. Tanner and J. Powell (1965). Gas lubricated bearings. *Journal of Applied Mechanics* 32 (3), 718.
- Guenat, E. and J. Schifmann (2019). Performance potential of gas foil thrust bearings enhanced with spiral grooves. *Tribology International* 131, 438-445.
- Lai, T., X. Peng, J. Liu, C. Guan, X. Chen, G. Tie and M. Guo (2019). Design optimization of high-precision aerostatic equipment based on orifice restriction. *Proceedings of the Institution of Mechanical Engineers, Part C: Journal of Mechanical Engineering Science* 233 (10), 3459-3474.
- Lu, Z. W., J. A. Zhang and B. Liu (2020). Research and Analysis of the Static Characteristics of Aerostatic Bearings with a Multihole Integrated Restrictor. *Shock and Vibration* 2020.
- Nishio, U., K. Somaya and S. Yoshimoto (2011). Numerical calculation and experimental verification of static and dynamic characteristics of aerostatic thrust bearings with small feedholes. *Tribology International* 44 (12), 1790-1795.
- Sahto, M. P., W. Wang, M. Imran, L. He, H. Li and G. Weiwei (2020). Modelling and simulation of aerostatic thrust bearings. *IEEE Access* 8, 121299-121310.
- Shah, T. R., H. M. Ali, C. Zhou, H. Babar, M. M. Janjua, M. H. Doranehgard, A. Hussain, U. Sajjad, C. C. Wang and M. Sultan (2022). Potential evaluation of water-based ferric oxide (Fe₂O₃-water) nanocoolant: An experimental study. *Energy* 246, 123441.
- Shao, J. P., G. D. Liu, X. D. Yu, Y. Q. Zhang, X. L. Meng and H. Jiang (2018). Effect of recess depth on lubrication performance of annular recess hydrostatic thrust bearing by constant rate flow. *Industrial Lubrication and Tribology* 70 (1), 68-75.
- Siddiqui, M., M. A. Azam and H. M. Ali (2022). Parametric evaluation of condensate water yield from plain finned tube heat exchangers in atmospheric water generation. *Arabian Journal for Science and Engineering* 47 (12), 16251-16271.
- Xiao, H., W. Li, Z. X. Zhou, X. M. Huang and Y. H. Ren (2018). Performance analysis of aerostatic journal micro-bearing and its application to high-speed precision micro-spindles. *Tribology International* 120, 476-490.
- Yan, R. Z., L. Y. Wang and S. Z. Wang (2019). Investigating the influences of pressure-

equalizing grooves on characteristics of aerostatic bearings based on CFD. *Industrial Lubrication and Tribology* 71 (7), 853-860.

Zhang, J. B., D. L. Zou, N. Ta and Z. S. Rao (2018). Numerical research of pressure depression in aerostatic thrust bearing with inherent orifice. *Tribology International* 123, 385-396.

Zhao, X. L., J. A. Zhang, H. Dong, Z. Fang and J. N. Li (2017). Numerical simulation and experimental study on the gas-solid coupling of the aerostatic thrust bearing with elastic equalizing pressure groove. *Shock and Vibration* 2017.